Dynamics and morphology characteristics of cell colonies with radially spreading growth fronts

M. A. C. Huergo,[1] M. A. Pasquale,[1] P. H. González,[2] A. E. Bolzán,[1] and A. J. Arvia[1]

[1]*Instituto de Investigaciones Fisicoquímicas Teóricas y Aplicadas (INIFTA) (UNLP, CONICET), Sucursal 4,*
Casilla de Correo 16, (1900) La Plata, Argentina

[2]*Cátedra de Patología, Facultad de Ciencias Médicas, Universidad Nacional de La Plata, Calle 60 y 120, (1900) La Plata, Argentina*

The dynamics of two-dimensional (2D) radially spreading growth fronts of Vero cell colonies was investigated utilizing two types of colonies, namely type I starting from clusters with a small number of cells, which initially exhibited arbitrary-shaped rough growth fronts and progressively approached quasicircular ones as the cell population increased; and type II colonies, starting from a relatively large circular three-dimensional (3D) cell cluster. For large cell population colonies, the fractal dimension of the fronts was $D_F = 1.20 \pm 0.05$. For low cell populations, the mean colony radius increased exponentially with time, but for large ones the constant radial front velocity 0.20 ± 0.02 μm min^{-1} was reached. Colony spreading was accompanied by changes in both cell morphology and average size, and by the formation of very large cells, some of them multinuclear. Therefore the heterogeneity of colonies increased and local driving forces that set in began to influence the 2D growth front kinetics. The retardation effect related to the exponential to constant radial front velocity transition was assigned to a number of possible interferences including the cell duplication and 3D growth in the bulk of the colony. The dynamic scaling analysis of overhang-corrected rough colony fronts, after arc-radius coordinate system transformation, resulted in roughness exponent $\alpha = 0.50 \pm 0.05$ and growth exponent $\beta = 0.32 \pm 0.04$, for arc lengths greater than 100 μm. This set of scaling exponents agreed with that predicted by the Kardar, Parisi, and Zhang continuous equation. For arc lengths shorter than 2–3 cell diameters, the value $\alpha = 0.85 \pm 0.05$ would be related to a cell front roughening caused by temporarily membrane deformations occasionally interfered by cell proliferation.

PACS number(s): 87.16.dj, 87.17.Ee, 87.18.Hf, 89.75.Da

I. INTRODUCTION

In recent years scientists from different areas of expertise became active in the investigation of laws and mechanisms related to the dynamics of different condensed phases comprising inorganic [1–3] and biological systems [4–11]. These studies, particularly those concerning living systems, require an interdisciplinary research approach in which areas of mathematics, physics, and biology are combined with the aim of developing models that could provide possible predictions to the behavior of real systems of medical interest.

The dynamics of different biosystems of increasing complexity has been studied from both the theoretical and the experimental standpoints. Growth processes in two-dimensional (2D) and three-dimensional (3D) biosystems have been described by a number of computer models and theoretical approaches [2,3,9,12,13]. These models are under constant revision as new properties of biosystems are discovered. In this regard, advances have been made either to compare experimental data based on the complex interactions involved in the dynamics of biosystems or to envisage possible classifications of growth patterns in terms of generic mechanisms of single cell dynamics at growth fronts [14–17].

Experimental work has focused on the study of growth pattern characteristics by the application of statistical thermodynamics to disorderly surface and phase growth, and their nonequilibrium roughening has been interpreted using scaling concepts to describe the growth dynamics in the presence of noise [2,8]. From the front roughness dependence on time and system size, a set of critical exponents, namely the global α, the local α_l and the spectral α_s roughness exponents, the growth exponent β, and the dynamic exponent $z = \alpha/\beta$ can be obtained. The validity of the set of critical exponents can be tested by either adequate rescaling arguments or renormalization group transformation so that the scaling functions collapse into a single curve. In simpler cases, when a congruent set of those exponents is obtained, it becomes possible to infer the likely universality class the condensed phase growth dynamics can be associated with [2,3]. Dynamic scaling analysis has been applied to growth front data from 2D bacteria [4] and cell line colonies [5,7], and 3D tumors [7]. However, the validity of conclusions derived from the analysis of radial growth front data, in terms of universality classes, has been extensively discussed [18,19]. The comparison of scaling analysis data derived from radially expanding systems to predictions from computational models of fixed size systems is still an open question [11,18–25].

In a recent paper, the 2D quasilinear growth of Vero cell colonies from initially quasistraight fronts was reported [26]. Vero cells were selected because they exhibit either a null or almost null contact inhibition, a typical property of cells in tumors, and continue growing and dividing indefinitely in vitro as long as adequate culture conditions are maintained [27]. Both the morphology features and dynamic scaling analysis of colony front data showed a complexity of the biological system that exceeded the framework of conventional condensed phase growth models, such as the continuous change of cell shape and average size distribution, the appearance of large, occasionally multinuclear, cells that resulted in a time-dependent heterogeneity of growing colonies, and the buildup of local driving forces contributing to the dynamics of the colony at a certain stage of growth. Under constant linear front velocity, the dynamic scaling analysis of quasi-2D fronts, within the 150–15000 μm size range, yielded the critical exponents $\alpha = \alpha_s = 0.5 \pm 0.05$ and $\beta = 0.32 \pm 0.04$. These figures, within

the experimental errors, fulfilled the Family-Vicsek relation and agreed with those predicted by the Kardar-Parisi-Zhang (KPZ) continuous equation. Although the KPZ model does not explicitly include most of the above-mentioned facts inherent to the colony front, it captures the essentials of the biosystem dynamics, in good agreement with the predictions of 2D cellular automaton models [10]. On the other hand, for colony front lengths shorter than 100 μm, the scaling behavior of the rough front appeared to be dominated by local cell deformations.

The above results suggested the convenience of investigating the radial spreading of Vero cell colonies to evaluate whether the preceding conclusions from 2D quasilinear growth fronts could be extended to 2D radial growth. This aprioristic question is not trivial since quasi-2D straight-line colony fronts are constrained to advance almost perpendicularly to the initial front, whereas 2D radial ones are accompanied by a progressive expansion of the colony front.

Data reported in this work were derived from two types of experiments to follow both the morphology evolution of colonies and their 2D growth front kinetics. For this purpose runs were performed utilizing two types of colonies, namely type I colonies consisting of 2D clusters with a small population of cells, and type II colonies starting to grow from 3D clusters. Experimental data from colonies consisting of a relative small number of cells follow an exponential spreading regime, whereas for a population exceeding about 700–1000 cells, the 2D growth fronts exhibit a constant radial velocity. At this stage changes in cell shape and size contribute to building up cell local density, concentration, and pressure gradients in the colony that help radial growth. Likewise, the formation of 3D cell domains, under certain conditions, and the occasional detachment of cells from the colony are also observed. The experiments confirm the exponential radial growth crossing over a constant linear growth velocity regime that has been reported for different cell lines and tumor models [14,28–31]. In the case of Vero cells, the velocity retardation effect, which appears during the growth of the colony, can be assigned to several contributions that hinder the radial spreading of the 2D growth front. From the colony growth pattern morphology there is evidence of 3D domain formation in the colony bulk, a process that for 2D Vero cell growth likely plays a relevant role in the retardation effect.

For front sizes ranging from 100 μm upward, i.e., the cell colony domain, the dynamic scaling analysis of the entire quasi-2D front evolution indicates that the KPZ continuous equation captures the behavior of the biosystem spreading under constant radial velocity. On the other hand, the critical roughness exponent derived from front sizes below 100 μm, i.e., the local cell deformation domain, approaches roughness exponent values that have been reported for other biosystems [4,7] and predicted for a growing interface that fluctuates in random media [2].

II. EXPERIMENT

A. Cell colony growth procedures

Vero cells were cultured using Roswell Park Memorial Institute (RPMI 1640) medium containing 10% fetal bovine

serum (FBS) maintained in a 5% carbon dioxide controlled atmosphere at 37 °C, changing one half of the culture medium every 2 days. Colonies were prepared by shedding disaggregated cells (500–1000 cell ml^{-1}, passage 165–180) in Petri dishes producing a large number of small clusters on the bottom about 48 h later. Then, about 5–6 clusters from each Petri dish were selected at random to follow up their quasi-2D front evolution. These type I colonies exhibited an initial random geometry that progressively became a quasicircular one. These experiments allowed us to study the dynamics of colonies at the early stages of growth.

To investigate the spreading of relatively large 2D circular fronts, runs were made utilizing type II colonies. In this case, a type I colony was left growing until a 3D cell cluster of about 250–300 μm radius was formed at the colony center. Subsequently, the 3D cluster was carefully removed with a micropipette and transferred to a second Petri dish containing fresh culture medium. Eventually, the type II colony continued spreading from the rim of this 3D seed as a 2D domain (Fig. 1).

For both types of colonies, the study was continued for about 7–8 days as the colonies eventually collapsed with neighbor clusters growing at the same time. For type I colonies, neighbor clusters are already present from the very beginning due to the shedding procedure itself, whereas for type II colonies, neighbor clusters are presumably formed mostly by occasional cell detachment from 3D colony domains, as the cell-cell adherence energy there becomes weaker than the cell-substrate interaction energy [32–35].

Colony fixation and staining with May-Grünwald Giemsa was occasionally performed to improve the detection of large multinuclear cells and cell filopodia and to evaluate the statistical distribution of cell size in 2D growth patterns. The viability of cells was routinely checked using the exclusion Tripan-Blue test. Cell duplication was determined by labeling with proliferating cell nuclear antigen (PCNA).
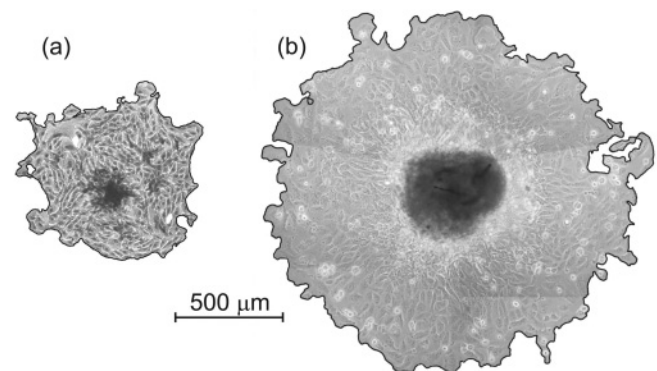

FIG. 1. Images of type I (a) and type II (b) colonies at advanced stages of growth. Type I colony, which has been fixed and stained, shows the formation of incipient 3D domains (black) in the bulk. Type II colony shows the growth of a large outer 2D domain and a thin 3D irregular-shaped ring starting from the rim of the 3D central core (black). Colony contours are highlighted. The scale length is indicated.
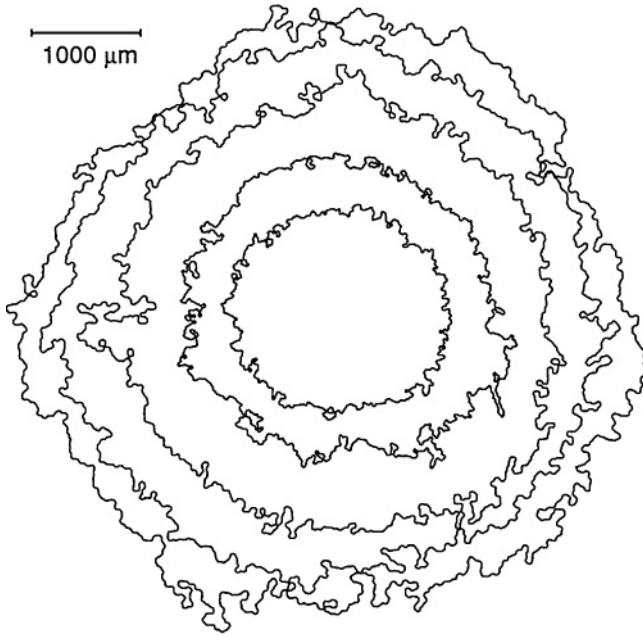
FIG. 2. Typical spreading of a colony front taken at 3120, 5400, 8520, 12 300, and 15 300 min. The length scale is indicated.

B. Colony imaging and data processing

Colony growth patterns were imaged daily using a Canon digital camera coupled to a Nikon TS100 phase-contrast inverted microscope with a CFI flat field ADL $10\times$ objective. The first image of each colony was taken at $t_0 = 2880 \pm 200$ min after seeding either cells or a 3D cell cluster. The entire image of each colony at time t resulted from the stitch and composition of a number of partial images with a resolution of 0.88 μm/pixel.

Colony fronts (Fig. 2) were manually traced using a Wacom graphic tablet. By conveniently zooming the images on the computer screen, the error of the traces was reduced to the order of the pixel. The analysis of the fronts was performed employing an in-lab developed program that provided the colony center of mass (c.m.), the instantaneous distance $R_i(t)$ from c.m. to the ith point at the front ($i = 1, 2, \ldots N$), the mean colony radius $\langle R \rangle$ ($\langle R \rangle = \sum R_i / N$), the mean radial front velocity $\langle v \rangle = d\langle R(t) \rangle / dt$, the instantaneous global roughness $w(L,t)$ at size L, and the colony front fractal dimension D_F.

The scaling analysis was performed by transforming the front coordinate system from angle radius into arc radius [7,8], so that the location of each point at the front was determined by coordinates s_i, R_i, the arc s_i being measured along the circle of radius $\langle R \rangle$ (Fig. 3). Hence for the front size L, the instantaneous global roughness of the expanding front was determined as the standard deviation of the radial fluctuations

$$w(L,t) = \left[\frac{1}{N} \Sigma [R_i(t) - \langle R(t) \rangle]^2 \right]^{1/2}. \qquad (1)$$

On the other hand, the local roughness of the front, $w(s,t)$, was evaluated from the standard deviation of radii R_i within an arc length s ($s < L$) at time t.

Global and local roughnesses were determined for both experimental and overhang-corrected data. The overhang-corrected profiles were obtained by taking the maximum value
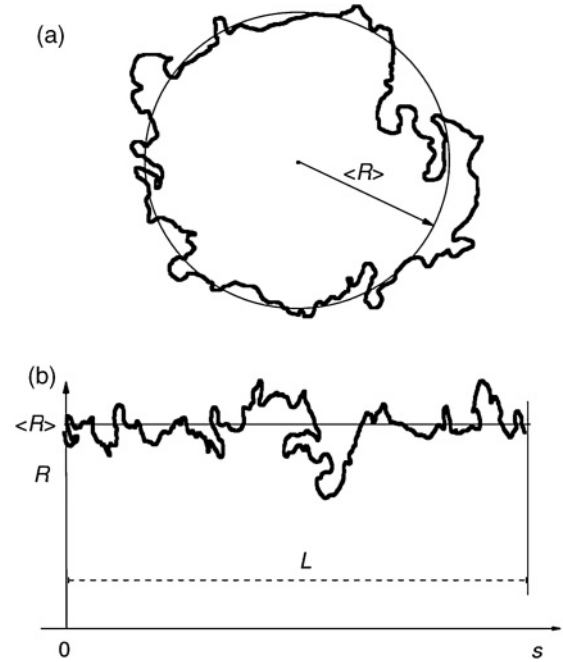

FIG. 3. (a) Scheme of a typical quasicircular 2D colony front of mean radius $\langle R \rangle$ measured with respect to the colony center of mass. (b) Linearized front resulting from the radius-angle to the radius-arc coordinate transformation.

of $R_i(t)$ for s_i in Fig. 3(b). As shown in the next section, the influence of overhang correction, required for scaling the front roughness, becomes practically null when s, the length of the colony front, exceeded the length of 3–4 average cell diameters.

III. RESULTS AND INTERPRETATION

A. Changes in the morphology of growing colonies

Type I colonies growing impromptu from a cluster of a few cells ($5 \leqslant n \leqslant 80$) had unpredictable shapes and their rough fronts showed irregularities such as protrusions and valleys, and some voids in the bulk (Fig. 4). However, despite the arbitrary initial shape of these colonies, once the population increased above 250 cells, they eventually acquired a quasicircular geometry (Fig. 5). This geometry appeared as a consequence of the random spatiotemporal duplication of cells without any predictable neighbor site location of each new cell in the cluster. The evolution of the shape of type I colonies was followed by its aspect ratio, defined by the major to the minor axis ratio of an ellipse with an area equivalent to that of the colony. As t increased, the aspect ratio became closer to 1 (Fig. 6). These plots show fluctuations in the aspect ratio value due to short time local random branching produced by cell duplication at the front. Conversely, type II colonies appeared quasicircular from the very beginning as the 2D radial displacement starts from the rim of the 3D cluster seed.

In general, the average cell size and shape, resulting from both types of colonies, depends on n, the cell population, and the colony age. Thus, for type I colonies consisting of a few cells, their average cell diameter is 40 ± 10 μm. As n increases, the average cell size decreases from the colony rim
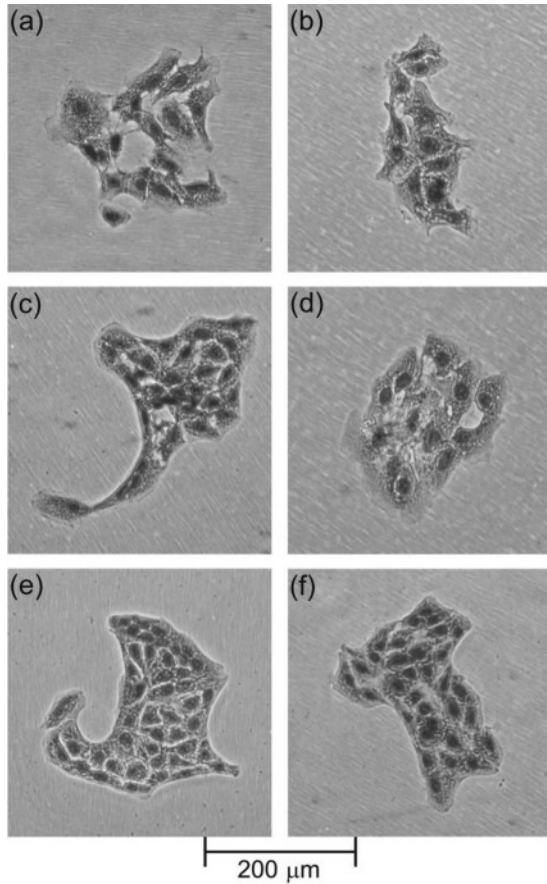
FIG. 4. Images of type I colonies at early stages of growth with different cell populations. For a better visualization of cells, colonies were fixed and stained with May-Grünwald Giemsa.

FIG. 6. Instantaneous aspect ratio versus growth time plots. Symbols correspond to different type I colonies. The dotted horizontal line indicates the circular front reference.

PCNA shows that cell proliferation takes place at both the rim and the bulk of the colony (Fig. 8).

For type I and II colonies and $t > 5000$ min, a relatively small number of large, some multinuclear, cells, and filopodia are formed, particularly at the colony front (Fig. 9). The origin of the large multinuclear cells, which have been reported elsewhere [36], is still unclear. These cell morphology changes modify the average cell size distribution at the colony front as seen in the corresponding histograms (Fig. 10); the skewness of the histograms moves from 1.6 to 2.7 in the interval

inward. At the innermost part of the colony the average cell size is about 50% their original size (Fig. 7). On the other hand, at sufficiently long times, some cells, particularly at the rim, reach diameters above 200 μm. Likewise, the number of voids in the bulk decreases and the local compactness of the colony increases. Furthermore, the labeling of growing colonies with
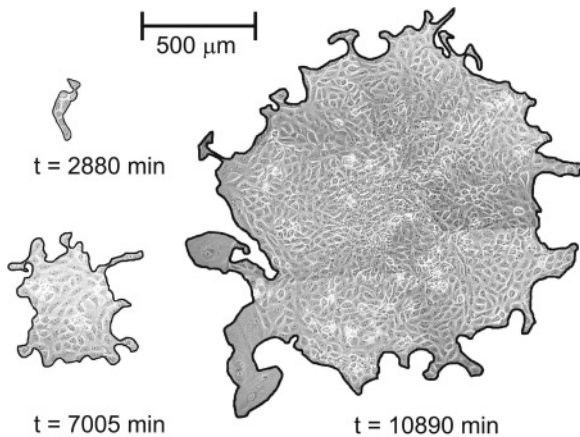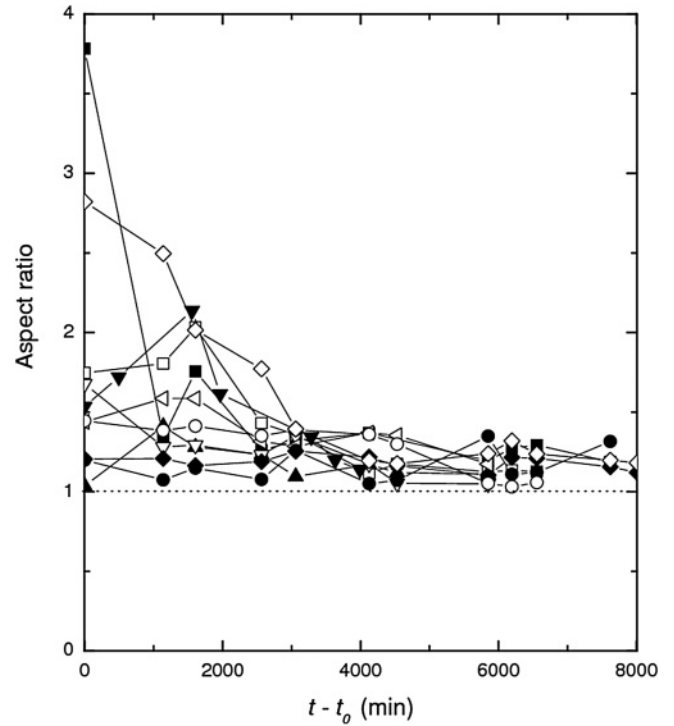

FIG. 5. Shape evolution of a type I colony from a quasilinear ($t = 2880$ min) to a quasicircular one ($t = 10\,890$ min). Colony fronts are highlighted and growth times are indicated.
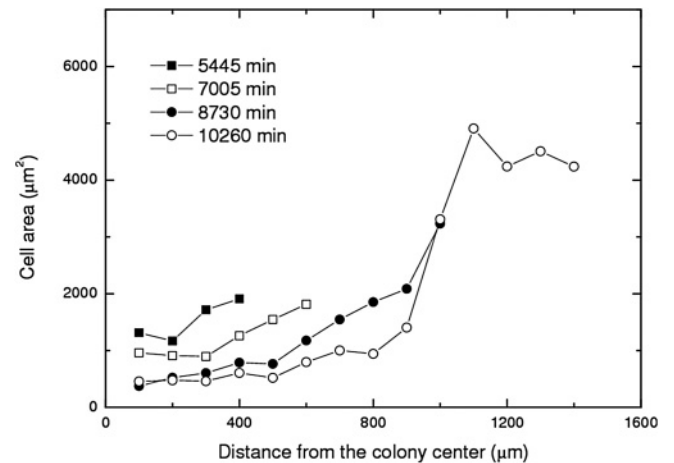

FIG. 7. Average cell area versus the radial distance from the center of a type I colony. Values were averaged from four equidistant colony radius. Colony growth times are indicated.
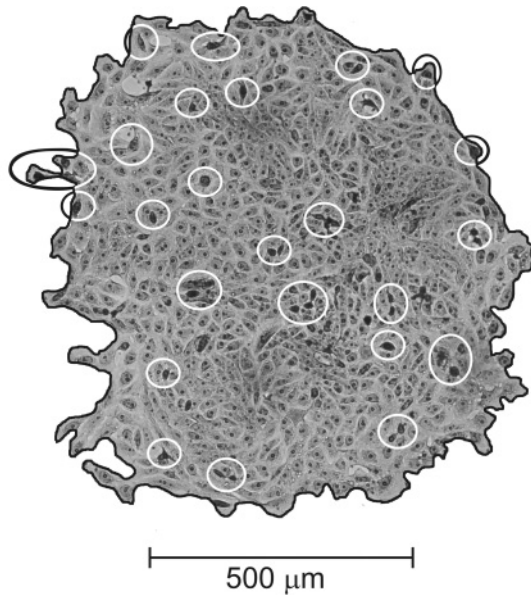
FIG. 8. Cell proliferation in a type I colony. The circles indicate cells that are positive for PCNA, i.e., those that are under mitosis at the time of labeling. For the sake of clarity, only some cells under duplication are indicated.

2880–13280 min, i.e., the greater t is, the broader the size distribution at the colony front results.

These changes result in a time-dependent heterogeneity of growing colony patterns, principally in the radial direction, which assist in the buildup of both local cell concentration and density gradients between the center and the front of the colony. They generate driving forces assisting mass transport and, at least in part, influencing 3D phase formation in the bulk of the colony [Fig. 1(a)].
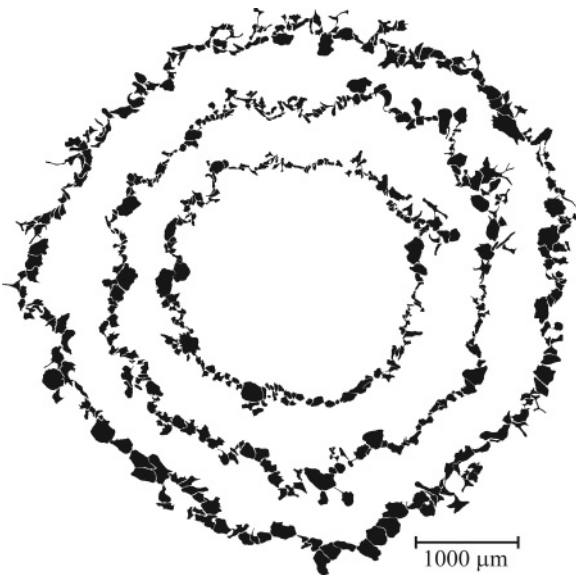

FIG. 9. Cell arrangement patterns at the rim of a type II colony at $t = 2880$, 5700, and 8880 min. The increasing contribution of large cells and filopodia with time can be observed. The scale length is indicated.
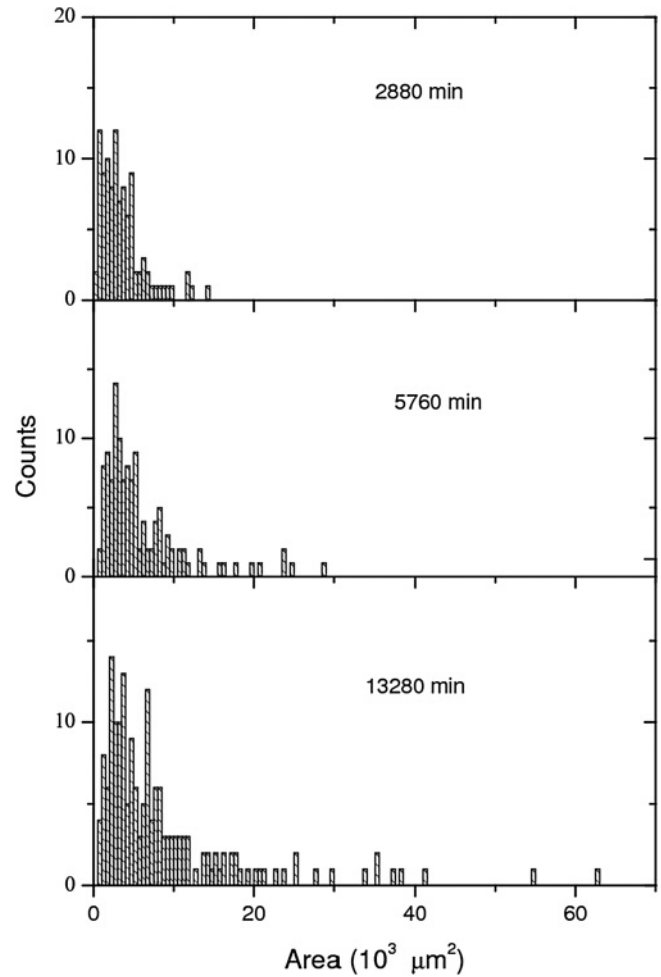

FIG. 10. Cell size histograms at the front of a type II colony for different times.

B. Colony growth kinetics

Colony growth kinetic data are obtained by cell counting from type I colonies. Unfortunately, for type II colonies, no reliable cell counting could be done because of the presence of the central 3D cell domain.

For type I colonies with a small initial number of cells (n_0), the instantaneous cell number $n(t)$ increases exponentially with t. Then, the increase in cell population can be expressed by a rate equation involving an average first order rate constant $\langle k_d \rangle$,

$$\frac{n(t)}{n_0} = e^{\langle k_d \rangle t}, \tag{2}$$

with $\langle k_d \rangle = 1/\langle \tau \rangle$, $\langle \tau \rangle$ being the average cell duplication time.

The normalized $\log(n/n_0)$ versus t plots approach a straight line with the average slope 2.2×10^{-4} min^{-1} (Fig. 11). From this figure, it follows that $\langle k_d \rangle = 5.2 \pm 0.7 \times 10^{-4}$ min^{-1} and $\langle \tau \rangle \approx 2000$ min, a value that is within the range of the Vero cell average duplication time reported elsewhere [37].

On the other hand, for type I colonies a linear $\log \langle R \rangle$ versus t plot results, the average slope being $1.02 \pm 0.02 \times 10^{-4}$ min^{-1} for $t < 9000$ min [Fig. 12(a)]. The deviation of data from linearity for $t > 9000$ min indicates a slower radial spreading velocity of the colony front. Conversely,
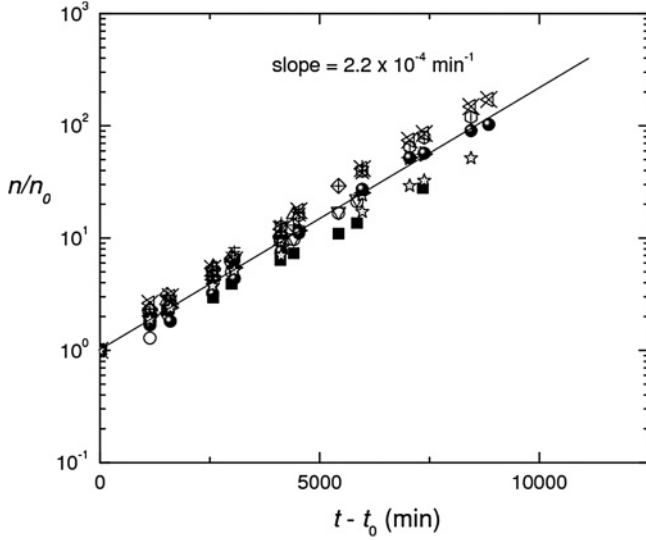
FIG. 11. Semilog normalized number of cells versus colony growth time plots [Eq. (2)] for type I colonies. Symbols correspond to different colonies.

type II colonies, growing around a 3D cluster seed of radius R_0, exhibit a linear $\langle R \rangle - R_0$ increase with t [Fig. 12(b)] with the slope $v_R = 0.20 \pm 0.02 \, \mu m \, min^{-1}$. This figure agrees with that previously reported for the 2D front velocity of Vero cell colonies started from quasilinear fronts [26].

Considering that for type I colonies with small n, both the instantaneous size and shape distribution of cells become fairly homogeneous, and further assuming that the colony geometry can be approximated to a circle of radius R, the instantaneous colony area [$A(t)$] can be related to $n(t)$ cells with the average radius r_c as follows:

$$A(t) = \pi R^2(t) = n(t)\pi \langle r_c \rangle^2. \tag{3}$$

Equation (3) predicts a linear R versus $n^{1/2}$ relationship that is observed from $n \to 0$ up to $n \approx 900$ (Fig. 13). For $n > 900$ experimental data deviate from Eq. (3) and the radial growth front velocity also deviates from the exponential regime [Fig. 12(a)].

Furthermore, as comes out from Eqs. (2) and (3), for type I colonies with $5 \leqslant n_0 \leqslant 90$, the 2D radial growth velocity data approach an exponential law (Fig. 14) resulting from

$$\frac{R(t)}{\sqrt{n_0} \, \langle r_c \rangle} = e^{\langle k_d \rangle t/2} \tag{4}$$

with a slope $1.1 \times 10^{-4} \, min^{-1}$, i.e., half the slope of Fig. 11, as expected.

The preceding analysis demonstrates the occurrence of two radial growth regimes that depend principally on the value of $n(t)$. Thus, for type I colonies, the lower $n(t)$ is the longer the exponential spreading regime results. The constant velocity regime is attained when n exceeds a value of 700–1000 cells. In contrast, for type II colonies, which involve large values of n from the very beginning, the constant radial growth velocity regime is already observed from $t \approx t_0$ upward [Fig. 12(b)].
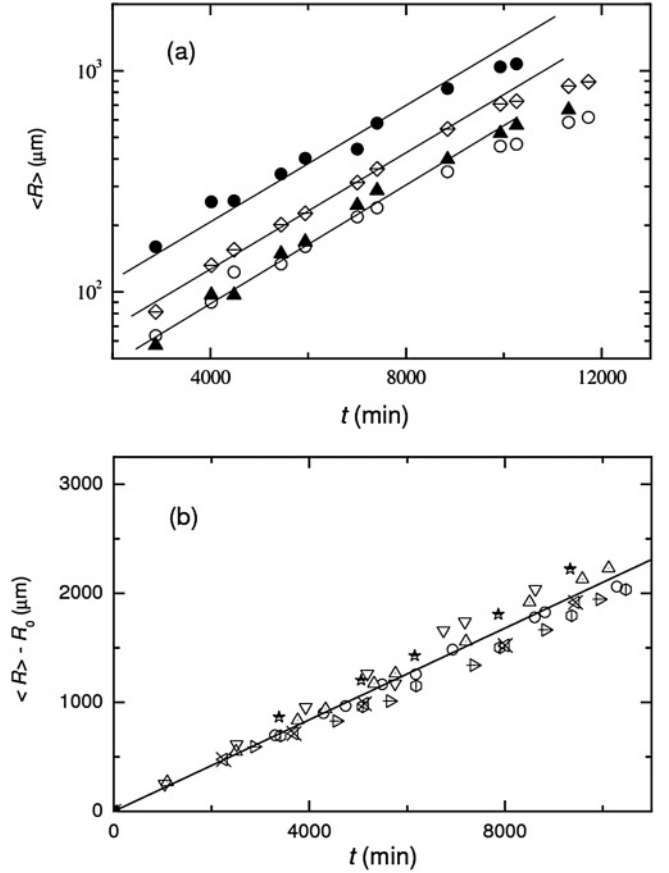

FIG. 12. (a) Log colony mean radius versus growth time plots for type I colonies. (b) 2D domain mean radius versus colony growth time plots for type II colonies ($R_0 =$ initial 3D cluster seed radius). Symbols correspond to different colonies.

IV. DYNAMIC SCALING ANALYSIS

The fractal dimension of colony fronts spreading at constant radial velocity, evaluated by the box-counting method, resulted in $D_F = 1.20 \pm 0.05$, a figure that agrees with values of D_F that have been obtained for Vero cell colonies under both quasilinear [26] and radial [7] growth. In contrast, for clusters with fronts far from circular, D_F was lower than 1.20. These
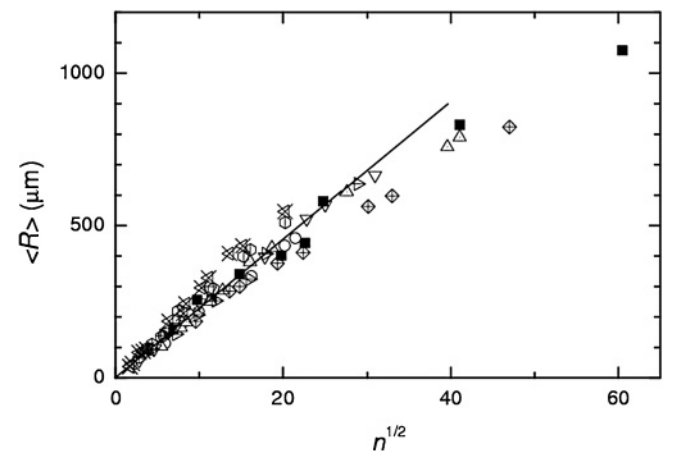

FIG. 13. Colony mean radius versus the square root of cell population plot. Symbols correspond to different type I colonies.
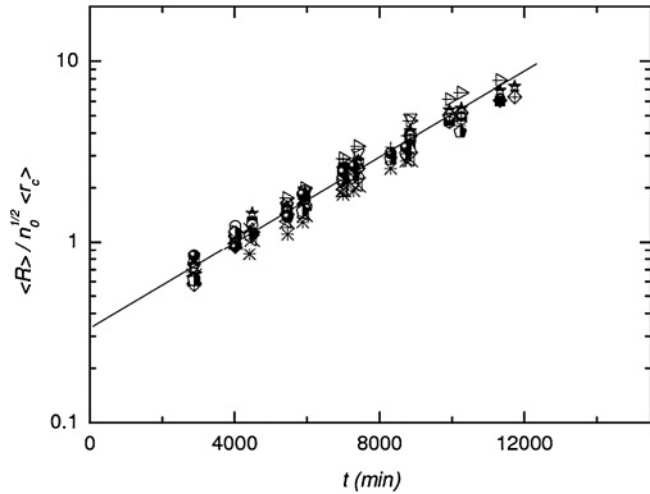
FIG. 14. Semilog plot of Eq. (4) for type I colony data for $\langle r_c \rangle = 15$ μm and $5 \leqslant n_0 \leqslant 90$.

values of D_F indicate complex colony contours with a low degree of ramification. Accordingly, the scaling analysis of radial colony fronts that spread at constant velocity was done
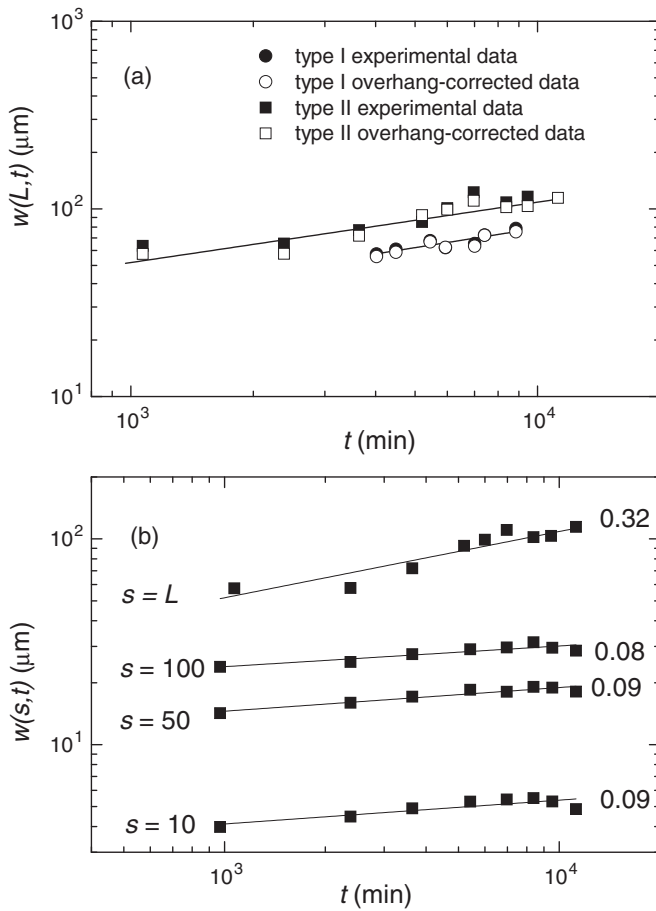

FIG. 15. (a) Front roughness versus growth time log-log plots for colonies of type I and II from both experimental and overhang-corrected data. (b) $w(s,t)$ versus t log-log plots from overhang-corrected data from type II colonies for different s values. Slope values are indicated on the right. For the sake of clarity, data have been binned.

by extending the validity of linear growth model equations to systems of increasing size [7,8,11,20,38] and transforming front coordinates from angle-radius to arc-radius ones (Fig. 3). This procedure has been utilized in the growth of plant callus [8] and a number of cell colonies and tumors [7].

A. Scaling exponents

According to the dynamic scaling theory [2], the roughness of a growing front of size L, $w(L,t)$, is expected to increase with t^{β} until it reaches a saturation value $w_s(L,t)$, the latter following a power law $w_s(L,t) \propto L^{\alpha}$. The roughness exponent α characterizes the stationary roughness regime in which the height-height correlation length has reached a value greater than L, while the growth exponent β accounts for the short time behavior of the growing front. Then, for a set of scaling exponents one expects the fulfillment of the Family-Vicsek relation [2]

$$ w(L,t) \propto L^{\alpha} f \left(\frac{t}{L^z} \right). \quad (5) $$

This approach has been applied to quasilinear single-valued fronts [26] and also tested for circular systems [21,39].

For roughness values measured along a colony front arc s relation (5) can be written as

$$ w(s,t) \propto s^{\alpha} f \left(\frac{t}{s^z} \right), \quad (6) $$
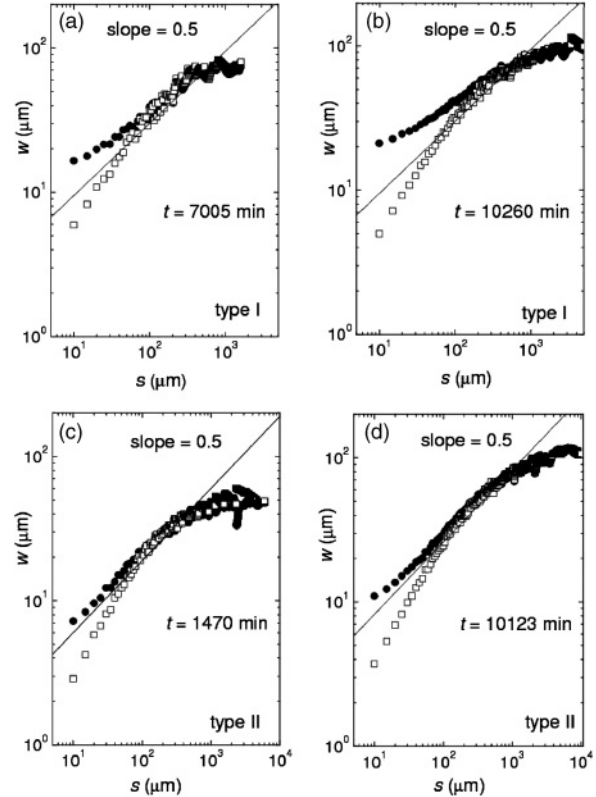
where $s < L$ (Fig. 3)

FIG. 16. Local colony front roughness versus arc length log-log plots. Data from type I (a), (b) and type II (c), (d) colonies at different times, as indicated. Black and open symbols correspond to experimental and overhang-corrected data, respectively.
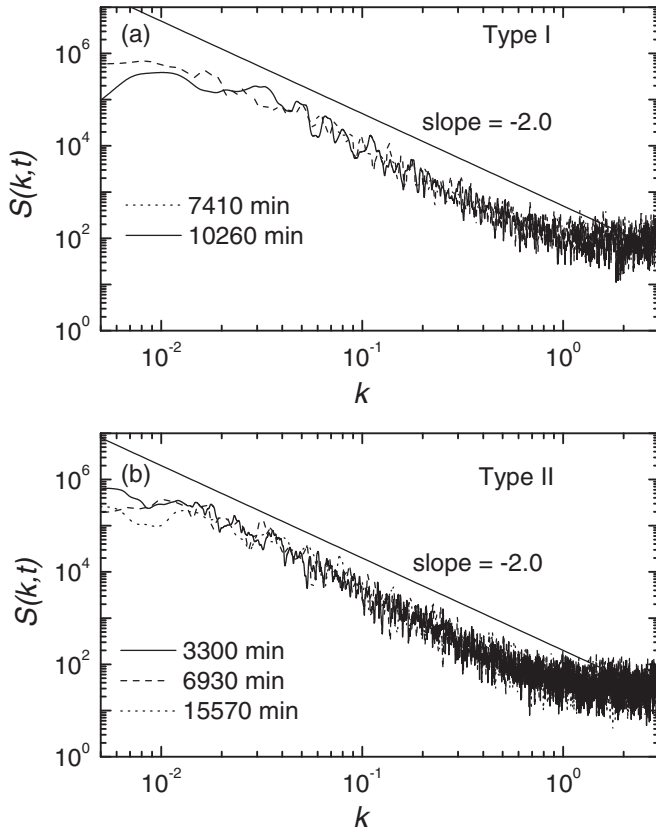
FIG. 17. Log-log plots of the structure factor for type I (a) and type II (b) colony front data at different times. The straight lines with a slope $-(2\alpha_s + 1) = -2$ are drawn to guide the eye.

Thus experimental and overhang-corrected front data from type I and type II colonies plotted as log $w(L,t)$ versus log t approach linear relationships with the same average slope $\beta = 0.32 \pm 0.04$ [Fig. 15(a)], covering about one decade of log t for type II colonies, and a shorter range for type I colonies. It should be noted that for the latter, the evaluation of β is constrained to colonies growing under constant radial velocity. In these cases, the average value of β agrees with that previously reported for Vero cell colonies approaching a quasilinear front [26]. On the other hand [Fig. 15(b)], the $w(s,t)$ versus t log-log plots, after overhang correction, in the range $10 \leqslant s \leqslant 100$, approach straight lines with very low slopes tending to zero, but when $s = L$, the slope results in 0.32.

The log $w(s,t)$ versus log s plots from experimental and overhang-corrected data (Fig. 16) collapse into a single curve for $s > s_0 \approx 100$ μm, irrespective of the type of colony. These plots indicate that the influence of overhangs on the front roughness becomes negligible when $s > s_0$, i.e., when s exceeds the length of about 3–4 cell average diameters. Data approach a linear region with a slope $\alpha \approx 0.5$ that extends for about one decade before local roughness saturation is attained, as expected for a system in the absence of global roughness saturation [26]. In contrast, for $s < s_0$, the plots of overhang-corrected data strongly deviate from the experimental roughness data, resulting in a straight line with a slope of about 0.85 (Fig. 16).

Therefore depending whether $s < s_0$ or $s > s_0$ one scales either the cell or the colony front domain, respectively. In general, the influence of overhangs on the radial growth front roughness appeared to be somewhat diminished as compared to quasilinear growth fronts [26], probably due to the increasing free space generated by the radial spreading of the colony.

A more generic scaling analysis can be obtained considering the structure factor $S(k,t)$ of the entire ($s = L$) growth front [2,10,40,41],

$$S(k,t) = k^{-(2\alpha_s+1)} f(kt^{1/z}),\tag{7}$$

with α_s being the spectral roughness exponent and $f(x = kt^{1/z})$ the scaling function, which depends on x as follows:

$$f(x) = \begin{cases} \text{const} & \text{for } x \gg 1; \\ x^{(2\alpha+1)} & \text{for } x \ll 1. \end{cases}\tag{8}$$

The advantage of estimating the scaling exponents in the Fourier space over real space methods is that only long wavelength modes contribute to the front scaling. Real space scaling [Eq. (6)] involves all wavelength modes, including short ones, so that stronger finite size effects should be expected.

The structure factor versus frequency log-log plots from overhang-corrected type I and type II colony front data (Fig. 17) approach a straight line with a slope close to
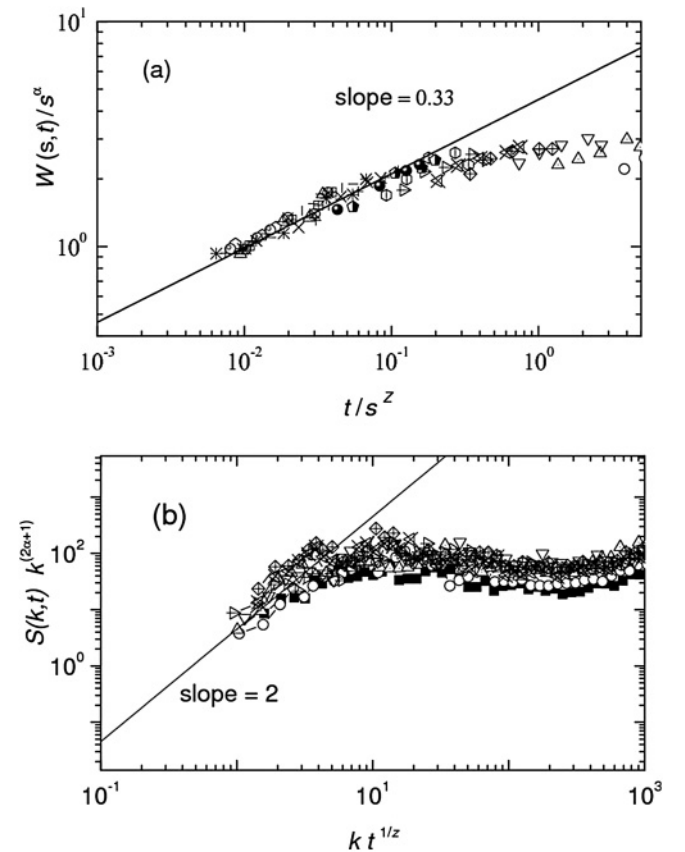

FIG. 18. Plots of Family-Vicsek scaling relationships [Eqs. (5) and (7)] for type I and type II colonies, considering $\alpha = 0.5$ and $z = 1.5$. Data have been binned for the sake of clarity.

-2.0 ± 0.1. Then, in the range $0.02 \leqslant k \leqslant 1$, $\alpha_s = 0.50 \pm 0.05$ results, irrespective of both t and the type of colony. Unfortunately, due to the noise of the system, no further conclusions about spectra displacement can be drawn from these plots, as one would expect if any anomalous scaling effect is involved [40].

The scaling exponents derived from the log-log plots of the dynamic scaling analysis (Figs. 15–17) were utilized to test the validity of the Family-Vicsek relation [42]. Thus both plots resulting from Eqs. (5) and (7) show reasonable collapses approaching a single universal curve (Fig. 18), in agrement with cell colonies starting from quasilinear 2D growth fronts [26].

V. DISCUSSION

A. Growth dynamics of clusters with a small number of cells

Radial spreading of cell clusters exhibiting arbitrary-shaped fronts consists of cells of rather homogeneous average size and shape. For these clusters, one should expect no appreciable influence of driving forces on the growth front displacement generated by concentration and density gradients in the colony, as occurs for colonies with large n reaching a quasicircular front. In this case, the average cell size at the front becomes greater than those of cells in the colony bulk at later colony growth stages. For these clusters a physical picture of the 2D front roughness evolution should consider at least two main contributions: one due to the random appearance of new cells, characterized by the average rate constant $\langle k_d \rangle = 5.1 \pm 0.7 \times 10^{-4}$ min^{-1}, and the other one related to local fast deformations of cell membranes. After cell duplication, the cluster front configuration depends on several possibilities of cell arrangements, some of them resulting in either void formations or lateral growth. The local fast deformation of cell membrane may also produce transient protrusions and cavities with small radii of curvature engendering a contribution to the front roughness, particularly significant for small clusters (Fig. 4). Consequently, the dynamics of clusters with small n largely depends on local stochastic processes associated with cell duplication and much faster cell membrane deformations.

B. Transition from exponential to constant radial growth front velocity

For a number of radially expanding cell line colonies, depending on their cell population, different growth kinetic regimes have been observed. It has been shown that, starting from a very low cell population, the colony mean radius increases exponentially with t, but once a certain value of n is exceeded, it continues growing at a constant radial velocity [7,28]. This velocity transition has been investigated utilizing computational models and interpreted in terms of sequential growth velocity regimes [28]. Accordingly, an initial diffusionlike growth regime obeying a $t^{1/2}$ power law (phase I) is expected only when the cell motility is high. Then, an exponential (phase II) velocity regime sets in and, finally, a crossover to linear growth in the asymptotic limit is attained. The appearance of this retardation effect has been assigned to a contact inhibition of cell division as the cell population increases [28]. Then, a scheme has been proposed consisting

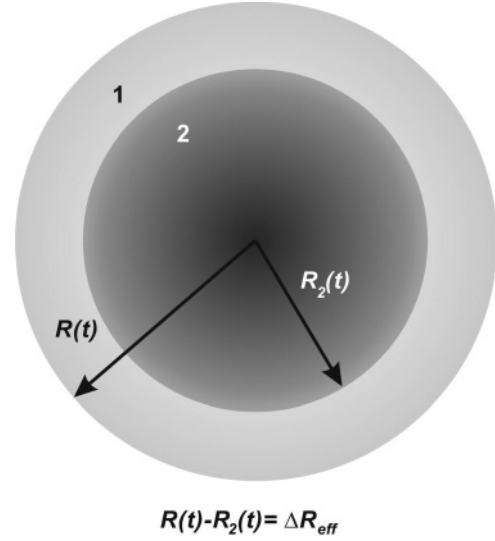$$R(t) - R_2(t) = \Delta R_{eff}$$

FIG. 19. Scheme of circular colony with a 2D proliferating cell domain that contributes to the expansion of the colony (light gray), and a central 3D domain that is related to a retardation effect (dark gray).

of a central core responsible for the retardation effect, and an outer ring of effective thickness where cell duplication occurs and contributes to the 2D expansion of the colony [28]. The growing colony cross section can be approached as an outer ring of effective thickness $\Delta R_{\text{eff}} = R(t) - R_2(t)$ and a central core of instantaneous radius $R_2(t)$ associated with the retardation effect (Fig. 19). Then, considering that at $t = 0$, $n = n_0$, and $R = R_0 < \Delta R_{eff}$, the transition from exponential to constant radial velocity regime has been expressed by the following equation [28]:

$$R(t) = \begin{cases} R_0 e^{(t/2\tau)}, & t \leqslant t_c, \\ \frac{\pi^{1/2} \Delta R_{\text{eff}}}{2}\left[1 + W\left(\frac{r_c^4 n_0^2}{\pi^2 \Delta R_{\text{eff}}^4} e^{(1+2t/\tau)}\right)\right], & t > t_c, \end{cases}$$

(9)

with $W(x)$ being the Lambert function and $t_c = \tau \ln(\Delta R_{\text{eff}}^2 / r_c^2 n_0)$. Then, as ΔR_{eff} attains a constant value the linear R versus t relationship is approached. By plotting our experimental data according to Eq. (9), considering $n_0 = 8$, a mean cell radius $r_c = 15$ μm, $\Delta R_{\text{eff}} = 330$ μm, and an average cell duplication time $\langle \tau \rangle = 2000$ min, they exhibit, within experimental errors, a reasonable agreement (Fig. 20). However, it should be noted that, despite this agreement, our results show that the phenomenology of colony growth exceeds the assumptions of the model. In fact, the transition from exponential to linear kinetic regimes appears accompanied by gradual changes in the colony features, such as (i) a change of the 2D front from an initially arbitrary to a quasicircular shape as n increases (Fig. 5); (ii) a decrease in the average size of cells in going from the colony front inward (Fig. 7); (iii) the appearance of 3D cell domains in the bulk of the colony [Fig. 1(a)]; (iv) the progressive formation of large cells, particularly at the colony rim (Fig. 9). Furthermore, the proliferation of cells occurs both at the rim and in the bulk of the colony (Fig. 8). Consequently, the slowdown of the 2D colony front radial displacement velocity, which has been attributed to contact inhibition of cell division, actually
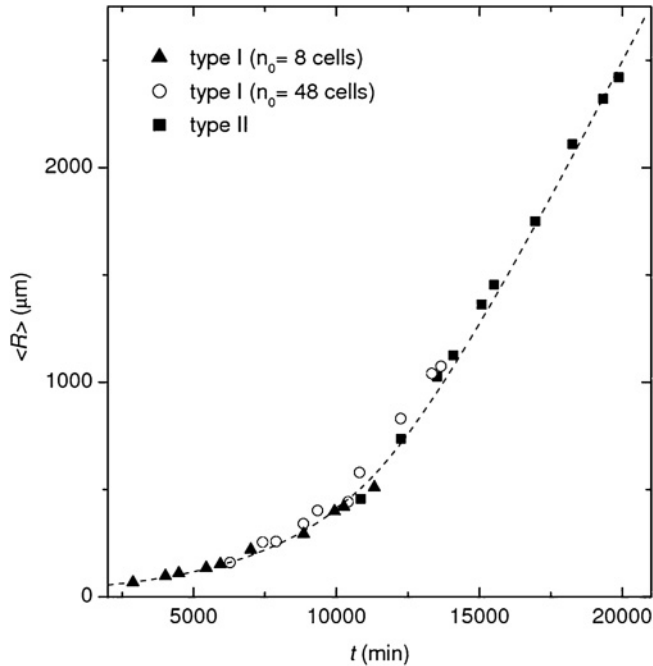
FIG. 20. Radial growth data of type I and II colonies. Data from type I colonies correspond to a different initial number of cells. The dashed trace corresponds to the plot of Eq. (9) for $n_0 = 8$, $r_c = 15$ μm, $\Delta R_{eff} = 330$ μm, and $\tau = 2000$ min.

involves a number of cooperative phenomena in which the complex mechanisms of each one of them involve biological and physicochemical interactions. For the case of Vero cells, the formation of 3D domains in the colony bulk likely plays a significant role in the retardation effect. This is in accordance with the fact that Vero cells exhibit either a null or almost null contact inhibition [27].

C. A likely interpretation of the dynamic scaling exponents

The dynamic scaling analysis of quasicircular growth front data allows us to distinguish two limiting scaling behaviors, depending on whether the front size is either lower or greater than the critical size $s_0 \approx 100$ μm, i.e., a size of about 3–4 cell diameters (Fig. 16). This behavior is comparable to that earlier described for the growth of colonies starting from quasilinear fronts [26] and shows that one can differentiate two scaling domains, one related to colony front fluctuations ($s > s_0$) and the other one where the roughness evolution would be dominated by the cell membrane properties ($s < s_0$).

For $s < s_0$ (cell domain), the scaling plots of overhang corrected data furnish the exponent $\alpha = 0.85 \pm 0.05$ (Fig. 16) and exponent $\beta \rightarrow 0$ [Fig. 15(b)]. The value of α is within the range of those that have been reported for bacteria growth ($\alpha = 0.75$) [4], burning fronts ($\alpha = 0.71$) [43], constant fluid flow in porous media ($\alpha = 0.81$) [44], paper wetting ($\alpha = 0.78$) [2], growth of some cell colonies and tumors ($\alpha = 0.9$) [7], and multiphase flow through a bead pack ($\alpha = 0.73$) [45,46]. For this case, a model has been proposed for linear front velocity displacement that involves surface tension, a pushing force, and temporarily quenched noise. It was expressed by a KPZ-like equation without its nonlinear term. Considering the system size and time range of

our experiments, a straightforward comparison of our data to those reported above is not feasible. Then, for the interpretation of exponents α and β for $s < s_0$ further research work has to be done. However, at this stage, we can admit that the value of α would be related to local cell membrane deformations occasionally perturbed by cell division, whereas exponent β indicates that in the smallest range of s the rate of roughness change becomes negligible.

For $s > s_0$ (colony domain), the influence of overhangs on the front roughness becomes negligible (Figs. 15 and 16), and the dynamic scaling and the Fourier analysis of roughness data result in the set of critical exponents $\alpha = 0.50 \pm 0.05$, $\beta = 0.32 \pm 0.04$, and $z = 1.50 \pm 0.2$, in agreement with the predictions of the KPZ equation. Therefore considering the reproducibility of data and the difficulty to obtain a more accurate collapse in the $S(k,t)k^{(2\alpha_s+1)}$ versus $kt^{1/z}$ log-log plots (Fig. 18), the fulfillment of the Family-Vicsek relation is acceptable. This set of KPZ exponents agrees with that previously reported for Vero cell colonies growing from 2D quasistraight linear fronts [26] and with the dynamic exponents derived from a cellular automaton model [10].

The KPZ behavior of growing 2D fronts of spreading condensed phases involves the participation of processes whose kinetics can be expressed by a general equation that contains linear, nonlinear and stochastic terms. The dynamics of 2D colony growth with a large cell population proceeds by a number of processes that can be described by linear differential equations such as those related to bulk diffusion, surface diffusion, surface tension and convective transport. On the other hand, biased displacement in the colony front, produced by the cell's own duplication and local cell deformations that contribute to the colony spreading, should also be responsible for a nonlinear help in the growth process. Finally, stochastic processes play a relevant role, principally in cell duplication. Therefore the entire colony growth process becomes extremely complex because it involves the concerted actions of biological constituents of the colony and the physicochemical properties of the whole biosystem, which in turn would depend on the age of the colony and the size and shape distribution of cells therein.

VI. CONCLUSIONS

The 2D radial front dynamics of Vero cell colonies consisting of a small number of cells follows an exponential law either in terms of n or R, but as n exceeds a critical value, a constant radial velocity is attained. This radial velocity transition is accompanied by gradual modifications of rough growth patterns, such as the evolution of small clusters from irregular to quasicircular colonies, the increase in the colony heterogeneity produced by the decrease in cell average size from the colony front inward, the appearance of large cells, and the progressive formation of 3D cell domains in the colony bulk. The change from the exponential to the linear 2D front radial velocity can be described assuming that at a long time, the colony spreading is due to the contribution of a proliferating ring around a central core hindering the 2D colony expansion [28]. However, this retardation effect cannot just be attributed to a contact inhibition process only, as cell duplication and 3D phase formation in the bulk of the colonies are observed.

The dynamic scaling analysis of colony fronts shows two limiting behaviors depending on whether the front size s is below or above a critical value $s_0 \approx 100 \ \mu$m. For $s < s_0$, the dynamic scaling analysis of the growth front implies contributions from both cell membrane deformations and the occasional interference of neighbor cell proliferation. In this range of s, the presence of overhangs strongly influences the front roughness value. The exponent $\alpha = 0.85 \pm 0.05$, obtained after overhang correction, is comparable to those earlier found for other biosystems. Furthermore, the value of β obtained for $s < s_0$ indicates that the rate of roughness change under these spatiotemporal conditions becomes negligible.

On the other hand, for $s > s_0$ the roughness evolution shows practically no influence of overhangs. The resulting critical exponents $\alpha = 0.50 \pm 0.05$, $\beta = 0.32 \pm 0.04$, and $z = 1.5 \pm 0.2$ are consistent with the KPZ universality class, and the set of critical exponents fulfill, within the experimental errors, the Family-Vicsek relation.

The agreement between the results reported here for 2D radially spreading growth fronts and those previously found for 2D quasilinear ones [26] indicates that the 2D growth front dynamics of Vero cell colonies fulfills the set of the scaling exponents derived from the KPZ continuous equation and agrees with the predictions of the cellular automaton model proposed earlier [10].

[1] M. Mandelbrot, *Fractal Geometry of Nature* (Freeman, San Francisco, 1982).

[2] A. L. Barabasi and H. E. Stanley, *Fractal Concepts in Surface Growth* (Cambridge University Press, Cambridge, England, 1995).

[3] P. Meakin, *Fractals, Scaling and Growth Far From Equilibrium* (Cambridge University Press, London, 1998).

[4] T. Vicsek, M. Cserzo, and V. K. Horvath, Physica A **167**, 315 (1990).

[5] A. Brú, J. M. Pastor, I. Fernaud, I. Brú, S. Melle, and C. Berenguer, Phys. Rev. Lett. **81**, 4008 (1998).

[6] M. T. Santini and G. Rainaldi, Pathobiology **67**, 148 (1999).

[7] A. Brú, S. Albertos, J. L. Subiza, J. L. García-Asenjo, and I. Brú, Biophys. J. **85**, 2948 (2003).

[8] J. Galeano, J. Buceta, K. Juárez, B. Pumariño, J. de la Torre, and J. M. Iriondo, Europhys. Lett. **63**, 83 (2003).

[9] H. M. Byrne, T. Alarcon, M. R. Owen, and P. K. Maini, Philos. Trans. **364**, 1563 (2006).

[10] M. Block, E. Schöll, and D. Drasdo, Phys. Rev. Lett. **99**, 248101 (2007).

[11] J. M. Pastor and J. Galeano, Cent. Eur. J. Phys. **5**, 539 (2007).

[12] H. P. Greenspan, Stud. Appl. Math. **51**, 317 (1972).

[13] A. R. A. Anderson, M. A. J. Chaplain, and K. A. Rejniak, *Single-cell-based Models in Biology and Medicine*, edited by A. R. A. Anderson, M. A. J. Chaplain, and K. A. Rejniak (Birkhäuser Verlag AG, Basel, 2007).

[14] D. Drasdo and S. Höhme, Phys. Biol. **2**, 133 (2005).

[15] I. Ramis-Conde, M. A. J. Chaplain, A. R. A. Anderson, and D. Drasdo, Phys. Biol. **6**, 016008 (2009).

[16] H. M. Byrne and D. Drasdo, J. Math. Biol. **58**, 657 (2009).

[17] J. Galle, M. Hoffman, and G. Aust, J. Math. Biol. **58**, 261 (2009).

[18] J. Buceta and J. Galeano, Biophys. J. **88**, 3734 (2005).

[19] A. Brú, Biophys. J. **88**, 3737 (2005).

[20] S. C. Ferreira and S. G. Alves, J. Stat. Mech. (2006) P11007.

[21] B. Brutovsky, D. Horvath, and V. Lisy, Physica A **387**, 839 (2008).

[22] C. Escudero, Phys. Rev. Lett. **100**, 116101 (2008).

[23] J. Krug, Phys. Rev. Lett. **102**, 139601 (2009).

[24] C. Escudero, Phys. Rev. Lett. **102**, 139602 (2009).

[25] C. Escudero, Cond. Mat. Stat. Mech., e-print arXiv:0912.2717.

[26] M. A. C. Huergo, M. A. Pasquale, A. E. Bolzán, A. J. Arvia, and P. H. González, Phys. Rev. E **82**, 031903 (2010).

[27] R. Sheets, *History and Characterization of the Vero Cell Line*, Technical Report (FDA, 2000).

[28] M. Radszuweit, M. Block, J. G. Hengstler, E. Schöll, and D. Drasdo, Phys. Rev. E **79**, 051907 (2009).

[29] J. P. Freyer and R. M. Sutherland, J. Cell. Physiol. **124**, 516 (1985).

[30] J. P. Freyer and R. M. Sutherland, Cancer Res. **46**, 3504 (1986).

[31] S. A. Menchón and C. A. Condat, Phys. Rev. E **78**, 022901 (2008).

[32] E. Paluch, J. van der Gucht, and C. Sykes, J. Cell Biol. **175**, 687 (2006).

[33] M. Aubert, M. Badoual, S. Féreol, C. Christov, and B. Grammaticos, Phys. Biol. **3**, 93 (2006).

[34] Y.-S. Chu, O. Eder, W. A. Thomas, Y. Sincha, F. Pincet, A. Ben-Ze'ev, E. Perez, J. P. Thiery, and S. Dufour, J. Biol. Chem. **281**, 2901 (2006).

[35] T. Rosen and D. S. Misfeldt, Proc. Natl. Acad. Sci. USA **77**, 4760 (1980).

[36] V. Kumar, A. K. Abbas, N. Fausto, and J. C. Fausto, *Patología Estructural y Funcional*, 8th ed. (Elsevier, Barcelona, 2010).

[37] A. T. Nahapetian, J. M. Thomas, and W. G. Thilly, J. Cell. Sci. **81**, 65 (1986).

[38] E. W. Kuennen and C. Y. Wang, J. Stat. Mech. (2008) P05014.

[39] A. Brú, D. Casero, S. de Franciscis, and M. A. Herrero, Math. Comp. Model. **47**, 546 (2008).

[40] J. J. Ramasco, J. M. López, and M. A. Rodríguez, Phys. Rev. Lett. **84**, 2199 (2000).

[41] J. M. López, M. A. Rodríguez, and R. Cuerno, Phys. Rev. E **56**, 3993 (1997).

[42] F. Family, Physica A **168**, 561 (1990).

[43] J. Zhang, Y. Zhang, P. Alstrøm, and M. T. Levinsen, Physica A **189**, 383 (1992).

[44] V. K. Horvath, F. Family, and T. Vicsek, J. Phys. A **24**, L25 (1991).

[45] D. A. Kessler, H. Levine, and Y. Tu, Phys. Rev. A **43**, 4551 (1991).

[46] M. A. Rubio, C. A. Edwards, A. Dougherty, and J. P. Gollub, Phys. Rev. Lett. **63**, 1685 (1989).